Available online at www.sciencedirect.com
SCIENCE DIRECT®
ELSEVIER
Ultramicroscopy 100 (2004) 331–338
ultramicroscopy
www.elsevier.com/locate/ultramic

Investigation of the surface structure and elastic properties of calcium silicate hydrates at the nanoscale

Cédric Plassard[a], Eric Lesniewska[a,*], Isabelle Pochard[b], André Nonat[b]

[a] *Physics Laboratory LPUB, UMR CNRS 5027, University of Bourgogne, F-21078 Dijon, France*
[b] *Chemistry Laboratory LRRS, UMR CNRS 5613, University of Bourgogne, F-21078 Dijon, France*

Received 1 June 2003; received in revised form 27 November 2003; accepted 28 November 2003

Abstract

This work is the first step towards the understanding of the structure of calcium silicate hydrate (C–S–H), the main constituent of cement paste, at the nanoscale. The first demonstration of atomic-resolution imaging of the (C–S–H) surface with an atomic force microscope (AFM) was performed.

C–S–H nanoparticles ($60 \times 30 \times 5\,nm^3$) were partially recrystallized by Ostwald ripening after long-term equilibrium in saturated calcium hydroxide solution of different concentration, leading to C–S–H of different calcium/silicon ratio (Ca/Si). The results of atomic resolution made possible the investigation of the C–S–H cell surface parameters. The surface layer structure depended on the calcium hydroxide concentration with which it equilibrated.

The change in structural properties perpendicular to the C–S–H layer was probed by modifying AFM for nanoindentation hardness measurements with a depth of indentation as low as 1 nm. The change in elastic modulus depending on the calcium/silicon ratio was evaluated and correlated in the change in structural parameters in this direction as estimated by X-ray diffraction.

PACS: 68.37.Ps; 62.20.Fe; 61.46.+w

Keywords: Atomic force microscopy; Surface structure; Nanoindentation; Elasticity; Nanophase materials

1. Introduction

Calcium silicate hydrate (C–S–H) is the main hydration product of Portland cement (in cement chemistry notation C, S and H refer to CaO, SiO_2, H_2O respectively). It precipitates from the dissolution of tricalcium and dicalcium silicates but is also formed by reactions between silica (for example, silica fume) and the rich calcium hydroxide interstitial solution. In special conditions, it also forms from reactions between calcium salt and alkaline silicate solutions.

In cement paste, C–S–H presents only a short-range crystalline order [1,2]; this is due to its nanocrystalline character [3,4]. Only a few

*Corresponding author. Tel.: +33-380-396034; fax: +33-380-396024.
E-mail address: lesniew@u-bourgogne.fr (E. Lesniewska).

0304-3991/$ - see front matter © 2004 Elsevier B.V. All rights reserved.
doi:10.1016/j.ultramic.2003.11.012

investigation techniques, such as Magic Angle Spinning Nuclear Magnetic Resonance (NMR) [5–8] and X-ray absorption spectroscopy applied to calcium [9,10], are adapted to the study of such materials. These techniques have made it possible to partly elucidate the crystalline structure of C–S–H. Therefore, the crystalline structure of C–S–H is not fully understood, although it is agreed that it presents a layered structure close to that of tobermorite, which is a rare mineral [11]. It is formed by the succession of layers consisting of a central part of calcium ions coordinated to half of the oxygen atoms of the silicate chains which form ribs covering each surface. The structure of the silicate chains is the repetition of a pattern of three tetrahedra (dreierket): two are paired and one forms the link between two adjacent pairs (bridging tetrahedron) (Fig. 1a). Some bridging tetrahedra may be missing. The other two oxygen atoms of each silicate tetrahedron may either be held in common with a silicate neighbour, or form a bond with a proton (silanol group) or a calcium ion in the interlayer. Moreover, it is established that its stoichiometry changes with the calcium hydroxide concentration in solution with which it equilibrates. Its calcium-to-silicon ratio (Ca/Si) then varies between 0.66 and 2 when the calcium hydroxide concentration varies from less than 1 to more than 30 mmol/l [12]. The ^{29}Si NMR showed

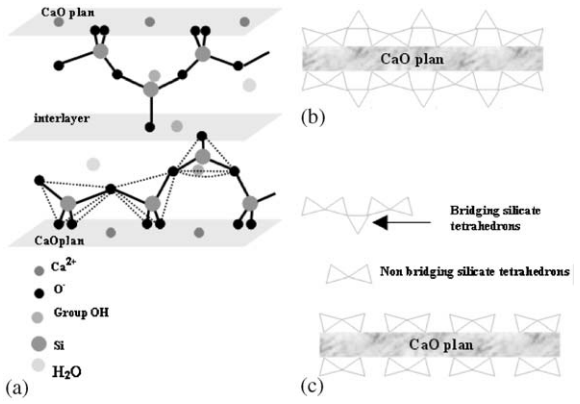

Fig. 1. Layered structure of C–S–H. (a) "Dreierketten" structure of silicate tetrahedra C–S–H. (b) Simplified diagram of C–S–H with infinite silicate chains (low lime concentration). (c) Simplified diagram of C–S–H with only dimeric silicate tetrahedra (high calcium hydroxide concentration).

that the length of silicate chains was variable [6,8,9]. Thus, when C–S–H equilibrates with low calcium hydroxide concentration, typically less than 1 mmol/l, the chains of silicate tetrahedra are infinite (Fig. 1b) and the Ca/Si ratio is equal to 0.66; C–S–H structure is the same as tobermorite structure [13]. An increase in calcium hydroxide concentration leads to the formation of dimers (Fig. 1c). The progressive rupture of the chains takes place by elimination of the bridging tetrahedra.

The origin of the cohesion of cement paste through the formation of C–S–H is the object of few studies [14] compared to those devoted to the hydration of cement, to the microstructure and strength of hardened pastes. Atomic force microscopy (AFM) already contributed significant input in this area and especially in the measurement of the interaction forces between C–S–H particle surfaces [15–18] and in the imaging of the growth of C–S–H. The formation of C–S–H on flat surfaces has been studied by AFM in each case, on alite, silica glass and calcite surface. In all cases, C–S–H precipitates on the surface by first forming an orientated aggregation of identical thin nanoparticles, the plane of the layers being parallel to the plane of the substrate [3,4,18]. In the case of the C–S–H coverage onto single calcite crystals, in which the substrate does not react in the equilibrium solution of C–S–H, a long equilibrium time allowed partial recrystallization. Micrometric atomically smooth domains were thus revealed [18]. With such atomically flat areas, atomic resolution made possible the investigation of the C–S–H surface structure which depends on the calcium hydroxide concentration in the equilibrium solution corresponding to the typical evolution of the Ca/Si ratio. The user of AFM was faced with the challenge of investigating the structural properties of C–S–H based on the atomic resolution of the surface of the layer. In order to probe the structural properties in the direction perpendicular to the plane of the layers, we studied elastic properties. Indeed, with an AFM, it is possible to measure the elastic modulus by AFM nanoindentation [19–21]. These spectroscopy modes reveal local elasticity variations [20].

2. Material and methods

2.1. Experimental setup

All experiments were performed into a glove box free from carbon dioxide to prevent carbonation of hydroxide solutions. Inside, a multimode AFM (Nanoscope IIIa; Veeco Co., CA) equipped with different scanners (0.8–150 μm) was operated in contact mode. The microscope was kept at over 80% relative humidity under a glass bell-jar by passing a decarbonated flux of dry nitrogen gas through calcium hydroxide solution. For studies in aqueous solutions, an adapted commercial fluid cell associated with a fluid exchange system was used to maintain steady bulk concentrations for all diffusion processes acting on the C–S–H crystal. Freshly prepared calcium hydroxide solutions flowed through the fluid cell. The temperature of the surrounding wall was maintained at 25°C. We have used V-shaped silicon nitride cantilevers or rectangular silicon cantilevers with spring constants of 10–4000 mN/m as measured by resonance frequency method and a Young's modulus of about 440 Gpa.

2.2. Substrate preparation

C–S–H coverage was obtained by immersion of a single crystal of calcite in a concentrated sodium silicate solution (pH = 14.2). The most efficient choice for the initial surface on which to observe the growth of C–S–H, was the $[1\,0\,\bar{1}\,4]$ cleavage plane of optical-quality calcite. The following chemical reaction occurs:

$$CaCO_3 \rightarrow Ca^{2+} + CO_3^{2-}, \quad (1)$$

$$xCa^{2+} + 2(x-1)OH^- + H_2SiO_4^{2-} \rightarrow (CaO)_x - (SiO_2) - (H_2O)_y. \quad (2)$$

Silicate concentration was chosen in such a way to shift equilibrium to C–S–H precipitation. C–S–H precipitates on the calcite surface in the form of identical nanoparticles ($60 \times 30 \times 5\,nm^3$). To obtain a sufficient coverage of C–S–H, the reaction between the calcite and the sodium silicate solution must continue for about 1 week. Then, the C–S–H covered single calcite crystals are immersed in different calcium hydroxide solutions ($0 < [Ca(OH)_2] < 22$ mmol/l) for 1 month to obtain C–S–H of different stoichiometries. At least five different C–S–H crystals for each of the eight different concentrations were thus analyzed: 0.16; 0.36; 0.82; 1.84; 4.53; 10.31; 14.69; 19.13 mmol/l. For comprehensive clarity, we labelled each set of C–S–H crystal samples 1–8. The advantages of single calcite crystals are two-fold: the initial surface is atomically smooth and it is non-reactive when the sample is in contact with the different calcium hydroxide solutions which provide different C–S–H stoichiometries. After 1 month of equilibration in the calcium hydroxide solutions, micrometric atomically smooth domains (Fig. 2) appeared. It must be mentioned that C–S–H nanoparticles are still present in the lowest part of the sample. From these microdomains, atomic resolution can be obtained.

2.3. Nanoindentation

We performed nanoindentation on recrystallized C–S–H surfaces. For calibration, load frame compliance was performed by pushing AFM probe on a smooth sapphire sample. In this case, because the sample contact stiffness is much higher than the probe spring constant, no tip penetration

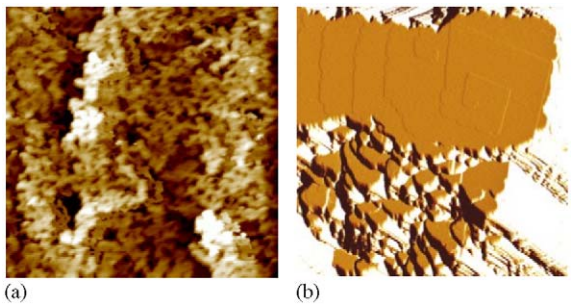

Fig. 2. C–S–H growth on the $\{1\,0\,\bar{1}\,4\}$ cleavage face of calcite. (a) Observation of several layers of C–S–H on calcite substrate after immersion in sodium silicate solution, which causes a rather significant roughness on the level of surface. Image size: $5 \times 5\,\mu m^2$. Relative height: 500 nm. (b) Observation of micrometric smooth domains of C–S–H recrystallized with crystalline growth into spiral shape after immersion in calcium hydroxide solution ($[Ca(OH)_2] = 19$ mmol/l), eliminating the effect of roughness. Image size: $5 \times 5\,\mu m^2$. Deflection: 0.1 nm.

occurs and the measured force–displacement response is characteristic of the given AFM probe. The probe response can be subtracted from the force–displacement responses measured on the C–S–H surface so that only the force–displacement response remains. Eight load levels ranging from 100 pN to 10 nN were used to indent the C–S–H surface. For each load level, 10 force curves were obtained on sapphire before and after indenting C–S–H sample, using the same probe and operating conditions. Smooth spline curves were fit to the unloading curves after successful attempts to get good fits using nonlinear power law fits and linear fits to logarithmic data. To use nanoindentation, we adapted an experimental device, allowing the application of normal force at the sample surface and chose cantilevers with higher stiffness constant in order to account for evolution of mechanical properties of C–S–H. With nanoindentation, we can follow the evolution of the force corresponding to the indentation applied; which differed according to the nature of the material. The studied samples showed behavior similar to that of mixed materials. To reach the elastic modulus, it was necessary to compare the results of various theories. By using two basic theories, these emerges a good interpretation. The amplified model of Hertz does not take into account the adhesion between tip and surface and considers an elastic sphere of radius R faces a rigid plan (C–S–H crystal):

$$E = \frac{3(1-v^2)k\,\Delta z}{4\delta^{3/2}R^{1/2}} \tag{3}$$

with v being Poisson's ratio, k the stiffness constant of AFM cantilever, Δz the displacement of the piezoelectric scanner and δ the indentation.

The other model used is the JKRS (Johnson Kendall Roberts Sperling) model, which neglects the long-range forces outside the contact area and considers only the short-range force inside the contact area [22]:

$$E = \frac{0.65k\,\Delta z - 3.28R^{3/4}k^{1/4}\,\Delta z^{1/4}F_{\mathrm{adh}}^{3/4}}{\delta^{3/2}R^{1/2}} \tag{4}$$

with F_{adh} being the adhesion force between tip and sample surface.

3. Results and discussions

3.1. Surface structure study of calcium silicate hydrates crystallized on calcite

Before claiming atomic resolution of C–S–H, it was necessary to calibrate the AFM in solution on standard samples such as freshly cleaved (0 0 1) face of the muscovite green mica (New York Co., New York, NY) and natural cleavage plane of calcite crystal. To avoid any ambiguity between resolutions on C–S–H crystals and the calcite substrate, we showed the atomic structure of the $\{1\,0\,\bar{1}\,4\}$ cleavage face of calcite ($CaCO_3$). Investigation of the calcite surface structure is carried out in aqueous environment (distilled water) in a controlled atmosphere. From atomic resolution (Fig. 3a), it was possible to obtain surface cell parameters by using the Fast Fourier Transform (FFT) (Fig. 3b), which provided the coordinates of atoms in the reciprocal lattice. The analysis of this FFT transform in the direct lattice gives access to the angle α and to the interatomic distances a and b (Fig. 3c), allowing the determination of the surface atomic lattice structure: $a = 8.20 \pm 0.13$ Å and $b = 5.15 \pm 0.08$ Å, angle $\alpha = 90°$. In the literature, it is reported that the calcite cell is close to the surface cell obtained here. Indeed, Stipp et al. [23] showed that atomic lattice of calcite was rectangular and the measured unit cell dimensions by AFM imaging in air was in good agreement with the LEED results for calcite surfaces ($a = 8.10 \pm 0.1$ Å and $b = 4.99 \pm 0.1$ Å). The parameters, being relatively close to the actual ones, authorize us to undertake the study of the C–S–H structure.

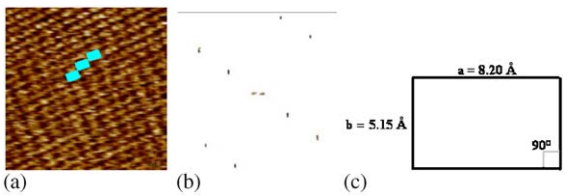

Fig. 3. Surface structure of the $\{1\,0\,\bar{1}\,4\}$ cleavage face of calcite $CaCO_3$. (a) Atomic resolution of calcite $CaCO_3$. Image size: $10 \times 10\,nm^2$. Relative height: 2 nm. (b) Fourier transform (FFT) of calcite. (c) Surface lattice of calcite $CaCO_3$.

The study was carried out, by considering samples equilibrated in increasingly concentrated calcium hydroxide solutions ranging from pure water (sample 1) to quasi-saturated calcium hydroxide solution [$Ca(OH)_2$] = 19 mmol/l (sample 8). The investigations carried out in electrolytic solution gave us the atomic resolutions presented in Fig. 4a, c, e and g. These atomic-resolution images exhibit the changes in the structure of the C–S–H surface according to the calcium hydroxide concentration in which it equilibrates. It seems

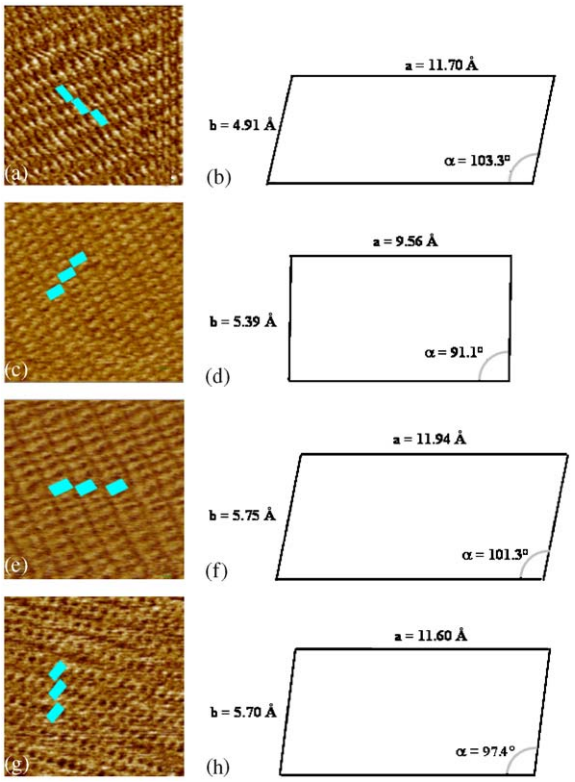

Fig. 4. Atomic resolution and surface cell of different samples. Surface structure of sample 1 (calcium hydroxide concentration = 0.16 mmol/l). (a) Atomic resolution. Image size: $10 \times 10\,nm^2$. Relative height: 1 nm. (b) Surface cell. Surface structure of sample 8 (calcium hydroxide concentration = 19.13 mmol/l). (c) Atomic resolution. Image size: $10 \times 10\,nm^2$. Relative height: 2 nm. (d) Surface cell. Surface structure of sample 5 (calcium hydroxide concentration = 4.53 mmol/l). (e) Atomic resolution. Image size: $10 \times 10\,nm^2$. Relative height: 2 nm. (f) Surface cell. Surface structure of sample 6 (calcium hydroxide concentration = 10.31 mmol/l). (g) Atomic resolution. Image size: $10 \times 10\,nm^2$. Relative height: 1.5 nm. (h) Surface cell.

that in the case of sample 1 (Fig. 4a), in which silicate chains should be parallel and infinite, only bridging tetrahedra were imaged by AFM. The pattern presented in the image corresponding to sample 8 (Fig. 4c) was very different; there were no more long chains of silicate tetrahedra. Although interpretation is difficult, the sample probably exhibits shorter chains. Intermediate samples (Fig. 4e and g) also show complex patterns intermediate between those of samples 1 and 8. From all these images, it was possible to obtain surface cell parameters starting from the angles and atomic coordinates giving by FFT. Surface cell parameters were obtained from analyses of more than 20 different areas per sample (five samples/calcium hydroxide concentration). The different lattices are given in Fig. 4b, d, f and h, and their values (and those at other concentrations) are reported in Table 1.

According to the measurements, by varying the calcium hydroxide concentration from 0.1 to 19 mmol/l, the angle between the lattice directions changed linearly. When the calcium hydroxide concentration was increased, the angle decreased (Fig. 5a). The amplitude of variation is as wide as a dozen degrees. This significant variation in the angle may be due to a sliding of the silicate chains in relation to each other.

Moreover, we also observed a modification in the cell surface parameters. Parameter *a* tends to increase slightly from sample 1 to sample 5 and to decrease afterwards. A notable reduction for sample 8 was observed (Fig. 5b). Parameter *b* sharply increases from sample 1 to sample 5, and then it decreases gradually (Fig. 5c). These changes in surface cell parameters and especially the decrease in *a* and *b* from sample 5 to sample 8 are probably due to the shortening of the silicate chains which occurs when the calcium hydroxide concentration increases. It would require a full interpretation of the image in terms of atomic position to completely understand these variations.

3.2. Nanoindentation on calcium silicate hydrates

Not being able to handle C–S–H crystals, we are not able to measure the bulk mechanical properties

Table 1
Surface cell parameters of C–S–H according to calcium hydroxide concentration

Sample	$[Ca(OH)_2]$ (mmol/l)	Parameter a (Å)	Parameter b (Å)	Angle α (°)
1	0.16	11.70 ± 0.18	4.91 ± 0.06	103.3 ± 0.2
3	0.82	11.75 ± 0.15	5.18 ± 0.05	102.4 ± 0.2
4	1.84	11.82 ± 0.19	5.53 ± 0.06	101.8 ± 0.1
5	4.53	11.94 ± 0.20	5.74 ± 0.07	101.1 ± 0.2
6	10.31	11.60 ± 0.12	5.70 ± 0.08	97.4 ± 0.1
7	14.69	10.64 ± 0.17	5.56 ± 0.07	94.4 ± 0.1
8	19.13	9.56 ± 0.11	5.39 ± 0.06	91.1 ± 0.1

The surface cell for sample 2 could not be given because of the mediocre quality of the resolutions obtained with this concentration. All solutions were saturated with respect to calcium silicate hydrate (C–S–H) by adding C–S–H powder to solutions and filtering them once equilibrium was reached.

by traditional techniques (oscillation, flexion). However, AFM allows measurement of the elastic modulus by nanoindentation.

In connection with the indentation depth (a few nanometers), we probed the mechanical properties of the C–S–H nanoparticules perpendicular to their developed face.

It was nonetheless necessary to first validate our experimental method. Knowing the theoretical elastic modulus calculated on the foshagite $Ca_4Si_3O_9(OH)_2$ by Laugensen [24], we indented this face perpendicularly. The foshagite, studied by X-ray diffraction [25], presents a monoclinic unit cell with lattice parameters: $a = 10.32$ Å, $b = 7.36$ Å, $c = 7.04$ Å, $\beta = 106.4°$. Let us look more closely at the (0 1 0) plan of the foshagite. The value of the Young's modulus is given by the formula:

$$E = \frac{\Sigma}{e}, \tag{5}$$

where Σ indicates the length of stress vector and e the length of applied strain vector.

Calculation leads to an elastic modulus perpendicular to the (0 1 0) plane of $E = 189.7$ GPa.

In experiments, the (0 1 0) plane of foshagite was indented in about 20 different areas with five measurements per area. The elastic modulus was then calculated by the Hertz and JKRS theories, and the average following results were obtained: $E_{Hertz} = 193.0 \pm 26.5$ GPa and $E_{JKRS} = 183.7 \pm 22.3$ GPa. In comparing the theoretical and experimental results, we noticed that the given elastic modulus was relatively closed.

The same control experiment was performed on the freshly cleaved (0 0 1) face of the muscovite green mica. The elastic modulus along the c-axis was estimated after 10 indentations. The values were: $E_{Hertz} = 49.9 \pm 1.5$ GPa and $E_{JKRS} = 46.2 \pm 1.4$ GPa. The elastic modulus measured by Vickers indentation was 48 GPa along the c-axis [26]. This validates our experimental procedure, based on the indentation of samples perpendicular to their surface. We could thus plan to reproduce these indentations on the C–S–H crystals.

The elastic moduli were averaged from 20 indentations per sample, carried out on several areas. Ten samples were analyzed after equilibrium with calcium hydroxide solutions of different concentration (the same solutions as used previously and others less concentrated). The results obtained were used to represent the characteristic of evolution of the elastic modulus according to the calcium concentration present in electrolytic solution (Fig. 6). Once again we noticed a different behavior between samples 1–5 and 6–8. The evolution of the elastic modulus largely follows two straight lines with different slopes. The slope of the first segment, corresponding to the solutions of weak concentrations of calcium, is the greatest, being characteristic of a fast evolution of the elastic modulus, up to a calcium concentration of about 8 mmol/l. We then noticed an inflection and the quasi stability of the elastic modulus for the highest calcium hydroxide concentrations ($[Ca^{2+}] = 19.13$ mmol/l, $E = 294.5 \pm 11.8$ GPa).

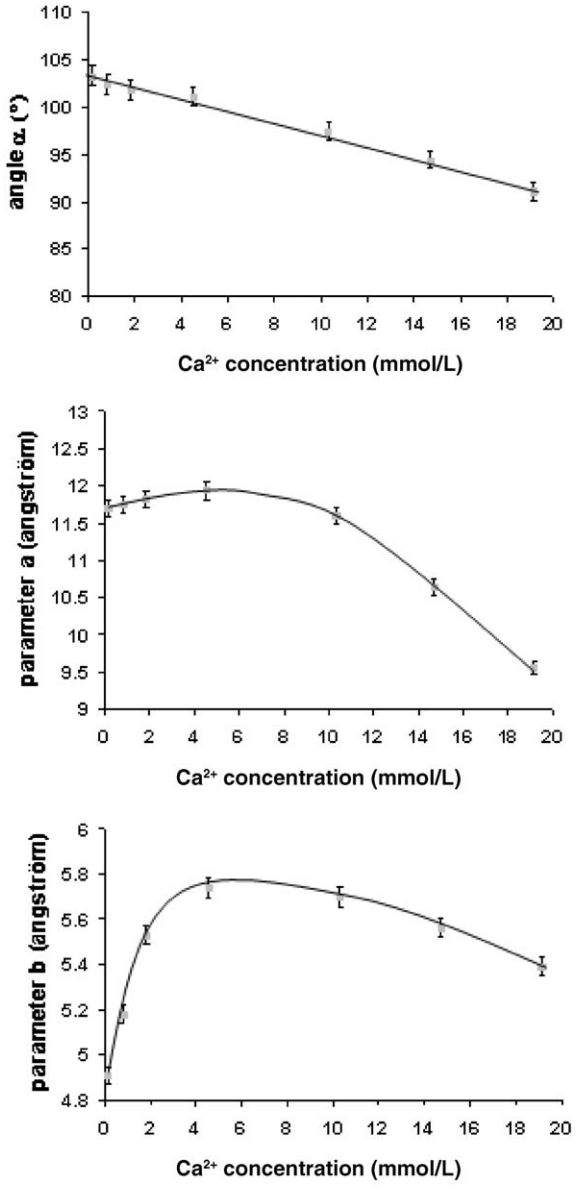

Fig. 5. Evolution of cell parameters according to calcium hydroxide concentration.

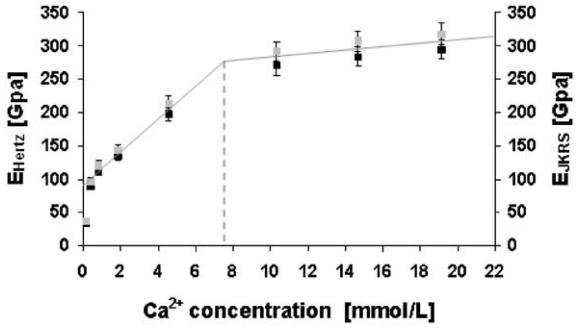

Fig. 6. Evolution of elastic modulus perpendicular to the C–S–H layer plane according to calcium hydroxide concentration.

In fact, the elastic modulus has been multiplied by almost 10 compared to the value obtained at low Ca^{2+} concentration ($[Ca^{2+}]=0.16$ mmol/l, $E=34.2\pm3.2$ GPa). This evolution of the elastic modulus may be related to the structural characteristics of the interlayer of C–S–H. For the lowest calcium hydroxide concentration, binding bounds of silicate tetrahedra are essentially silanol groups: the cohesion between the layers is due to silanol–water–silanol (OSiOH–H_2O–HOSiO) bonds. By increasing the calcium hydroxide equilibrium concentration, we expected a modification in the nature of the chemical bond. Indeed, silanol groups are increasingly ionized as the calcium hydroxide concentration increases and the negative charges created are balanced by Ca^{2+} ions in interlayer; the (OSiOH–H_2O–HOSiO) bonds are therefore replaced by an iono-covalant SiO^-–Ca^{2+}–SiO^- bond, causing a reduction in the interlayer space c between two calcium planes. In consequence, the compactness of C–S–H crystal cell increases and the elastic modulus rises by a factor 10. In addition, it has been shown, in the literature that the distance c between two Ca^{2+} planes as measured by X-ray diffraction declines sharply when the calcium hydroxide concentration increases [8]. These observations are in perfect agreement with the results revealed by nanoindentation. The results obtained at the calcium concentration $[Ca^{2+}]=0.36$ mmol/l ($E=88.9\pm4.9$ GPa) could be compared to the calculated elastic moduli of tobermorite [27]. The authors calculated the elastic modulus of a system based on independent tobermoritic layers (not chemically dependent). Only the deformations perpendicular to the interlayers were considered: the perpendicular elastic modulus was estimated equal to 81.0 GPa.

4. Conclusion

It has been possible to investigate the structural properties of C–S–H crystals supported by single calcite crystals with the aid of the AFM: in the topographic mode, we gained access to structural information concerning the plan $(\vec{a}, \vec{b})$, i.e. the plan of the layers of C–S–H, while with nanoindentation, we probed information accordingly concerning the axis $\vec{c}$, i.e. the direction perpendicular to the layers. Most of the atomic resolutions confirmed the ordered character of C–S–H and thus made it possible to determine the cell surface parameters of C–S–H. An increase in the calcium hydroxide concentration generates a decrease in the angle between the directions $\vec{a}$ and $\vec{b}$, and modifies the parameters a and b of the cell. This increase in calcium hydroxide concentration also influences the evolution of the elastic modulus. Indeed, we then expect a change in the nature of the chemical bonds, causing a reduction in the interlayer space c between two layers. Both elastic modulus and cell parameters show a discontinuity when the equilibrium concentration is about 8 mmol/l. This discontinuity may suggest a phase transition as has been suggested by other investigations [6,12].

Acknowledgements

We extend our most profound thanks to Dr. J.L. Laugensen and Dr. R.J.-M. Pellenq for fruitful discussions. This project is part of the Research Program Contract "Mechanic and Chemistry of Cement Materials" financially supported by CNRS and Association Technique des Industries des Liants Hydrauliques (ATILH). Cedric Plassard was supported by a scholarship from the ministry of research MENRT.

References

[1] D. Viehland, J.F. Li, L.J. Yuan, Z. Xu, J. Am. Ceram. Soc. 79 (1996) 1731.
[2] Z. Xu, D. Viehland, Phys. Rev. Let. 77 (1996) 952.
[3] S. Gauffinet, E. Finot, A. Nonat, Experimental study and simulation of C–S–H nucleation and growth, Proceedings of the Second International RILEM Symposium, RILEM Publications, 1997.
[4] S. Gauffinet, E. Finot, E. Lesniewska, A. Nonat, CR Acad. Sci. Paris 327 (1998) 231.
[5] J.F. Young, J. Am. Ceram. Soc. 118 (1988) 71.
[6] M. Grutzeck, A. Benesi, B. Fanning, J. Am. Ceram. Soc. 72 (1989) 665.
[7] D. Damidot, A. Nonat, P. Barret, D. Bertrandie, H. Zanni, R. Rassem, Adv. Cement Res. 7 (1995) 1.
[8] I. Klur, B. Pollet, J. Virlet, A. Nonat, NMR Spectroscopy of Cement Based Materials, Springer, Berlin, Heidelberg, 1998, p. 119.
[9] R.J. Kirkpatrick, G.E. Brown, N. Xu, X. Cong, Adv. Cement. Res. 9 (1997) 31.
[10] N. Lequeux, A. Morau, S. Philippot, P. Boch, J. Am. Ceram. Soc. 82 (1999) 1299.
[11] H.F.W. Taylor, J. Am. Ceram. Soc. 69 (1986) 464.
[12] A. Nonat, X. Lecoq, NMR Spectroscopy of Cement Based Materials, Springer, Berlin, Heidelberg, 1998, p. 197.
[13] S.A. Hamid, Z. Kristallogr. 154 (1981) 189.
[14] A. Nonat, J.C. Mutin, Hydration and Setting of Cements, Proceedings of the International RILEM, E&F Spon, London, 1991.
[15] E. Finot, E. Lesniewska, J.C. Mutin, J.P. Goudonnet, J. Chem. Phys. 111 (1999) 6590.
[16] E. Finot, E. Lesniewska, J.P. Goudonnet, J.C. Mutin, Appl. Surf. Sci. 161 (2000) 316.
[17] E. Finot, E. Lesniewska, J.P. Goudonnet, J.C. Mutin, M. Domenech, A.A. Kadi, Solid State Ionics 141 (2001) 39.
[18] S. Lesko, E. Lesniewska, A. Nonat, J.C. Mutin, J.P. Goudonnet, Ultramicroscopy 86 (2001) 11.
[19] S. Sundararajan, B. Bhushan, Sensors Actuators A 101 (2002) 338.
[20] B. Bhushan, Wear 251 (2001) 1105.
[21] M. Finke, J.A. Hughes, D.M. Parker, K.D. Jandt, Surf. Sci. 491 (2001) 456.
[22] K.L. Johnson, K. Kendall, A.D. Roberts, Proc. R. Soc. A 342 (1971) 301.
[23] S.L.S. Stipp, C.M. Eggleston, B.S. Nielsen, Geochim. Cosmochim. Acta 58 (1994) 3023.
[24] J.L. Laugensen, Private Communication.
[25] J.A. Gard, H.F.W. Taylor, Acta. Crystallogr. 13 (1960) 785.
[26] S. Habelitz, G. Carl, C. Rüssel, S. Thiel, U. Gerth, J.-D. Schnapp, A. Jordanov, H. Knake, J. Non-Cryst. Solids 220 (1997) 291.
[27] O. Rozenbaum, R.J.-M. Pellenq, A. Gmira, H. Van Damme, J. Phys. Chem., 2003, submitted.